Available online at www.sciencedirect.com
SCIENCE DIRECT®
Journal of Structural Biology 145 (2004) 142–151
Journal of Structural Biology
www.elsevier.com/locate/yjsbi

A binary segmentation approach for boxing ribosome particles in cryo EM micrographs

P.S. Umesh Adiga,[a,*] Ravi Malladi,[b] William Baxter,[c] and Robert M. Glaeser[a,d,*]

[a] *Physical Biosciences Division, LBNL, 1, Cyclotron Road, Berkeley, CA 94720, USA*
[b] *Computing Sciences Division, LBNL, 1, Cyclotron Road, Berkeley, CA 94720, USA*
[c] *Wadsworth Center, PO Box 509, Albany, NY 12201, USA*
[d] *Molecular and Cell Biology, University of California, Berkeley, CA 94720, USA*

Received 25 June 2003, and in revised form 10 October 2003

Abstract

Three-dimensional reconstruction of ribosome particles from electron micrographs requires selection of many single-particle images. Roughly 100,000 particles are required to achieve approximately 10 Å resolution. Manual selection of particles, by visual observation of the micrographs on a computer screen, is recognized as a bottleneck in automated single-particle reconstruction. This paper describes an efficient approach for automated boxing of ribosome particles in micrographs. Use of a fast, anisotropic non-linear reaction-diffusion method to pre-process micrographs and rank-leveling to enhance the contrast between particles and the background, followed by binary and morphological segmentation constitute the core of this technique. Modifying the shape of the particles to facilitate segmentation of individual particles within clusters and boxing the isolated particles is successfully attempted. Tests on a limited number of micrographs have shown that over 80% success is achieved in automatic particle picking.

Keywords: Micrograph; Particle; Diffusion; Segmentation; Boxing

1. Introduction

Electron microscopy (EM) techniques comprise a powerful and diverse collection of methods that facilitate visualization of biological structures at a macromolecular level. Electron microscopy covers a range of resolution that spans several orders of magnitude, bridging the gap between crystallography and light microscopy (Sali et al., 2003). The resolution of an image of macromolecular structures depends on the number of electrons applied to the sample, since a trade-off exists between statistical definition and damage to sample (Glaeser, 1971). Micrographs showing projections of macromolecular assemblies must be recorded at very low electron dose to minimize radiation damage, resulting in low image contrast (Henderson, 1995). Overcoming the limitations posed by the low electron exposures that are "safe" requires merging data from images of up to millions of molecules in order to increase the signal-to-noise ratio. The number of macromolecule images required for a volumetric reconstruction increases significantly with the resolution of the micrograph (Frank, 1996). When images of currently available quality are used, it is believed that at least one million particles are required to reconstruct a protein molecule with "atomic" resolution (Henderson, 1995; Sali et al., 2003).

For reconstructing the three-dimensional (3-D) shape of a protein molecule, particles from each micrograph are selected either manually, using interactive graphics software or by computer aided semi-automatic methods. Either method becomes a very labor intensive job when the number of particles required becomes very large. Automation of particle selection is hence necessary to prevent this stage from becoming a serious bottle neck in visualization of the structure of a protein molecule. Several approaches to automate particle picking have been proposed which have met with varying degrees of

* Corresponding authors. Fax: 1-510-4866199 (P.S. Umesh Adiga), 1-510-486-6488 (Robert M. Glaeser).
E-mail addresses: upadiga@lbl.gov (P.S. Umesh Adiga), rmglaeser@lbl.gov (R.M. Glaeser).

1047-8477/$ - see front matter © 2003 Elsevier Inc. All rights reserved.
doi:10.1016/j.jsb.2003.10.026

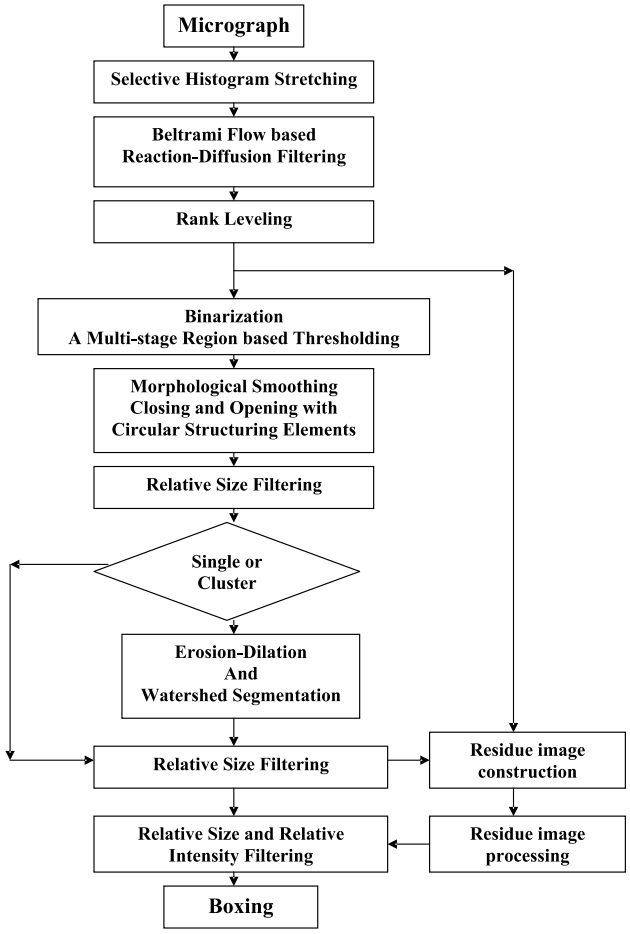

Fig. 1. Flow diagram of particle boxing process.

success (Nicholson and Glaeser, 2001). Among these, particle extraction based on texture features of candidate particles obtained by peak search of the Gaussian smoothed micrograph was proposed by Lata et al. (1995). Although this method remains one of the most effective that has been described to date, many false positives still get through and a manual editing of the resulting data is required as a final step.

In this paper, we present a methodology based on nonlinear preprocessing of micrographs followed by multilevel, region-based thresholding and morphological segmentation. Fig. 1 shows the flow diagram of various procedures integrated in a pipeline fashion for particle picking purpose. Our objective is not just extraction of single particles but also to segment those single particles which are located rather close to one-another, thus increasing the throughput of the boxing process without increasing erroneous selection of particles.

2. Segmentation of ribosome particle images

Micrographs of ribosome particles lack clarity and definition because of the high level of electron shot noise mentioned above (Glaeser, 1971). The design of computational techniques that can extract particles from the background and from interfering materials in the image is thus essential. Normalization of the micrographs to have approximately the same mean and grey-level distribution for all the micrographs, followed by an anisotropic reaction-diffusion and rank-leveling to smooth the background texture and to remove the illumination variation, constitute the pre-processing steps. Pre-processed micrographs are then thresholded and individual particles and clusters are separated. Particles within the clusters are then segmented by a combined erosion-dilation and region growing algorithm. This is followed by a second stage of particle picking and boxing of the segmented particles in the micrograph.

2.1. Pre-processing

When we digitize the micrographs, the measured optical density (OD) values reflect the electron image intensity at each point on the micrograph. Within a large data set, however, one can expect to have significant variations in the average electron intensity due to variations in specimen thickness from one micrograph to the next, variations in condenser lens setting, different choice of image magnification from one day to the next and other factors. Standardization of micrographs is thus essential. Standardization is done by selective histogram stretching. Selective histogram stretching consists of stretching only a selected part of the histogram that contains most of the pixels. The max and min values are defined as the grey-levels where the histogram curve falls to below 1% + offset and 1% − offset of the number of pixels at the mode point of the histogram on both sides of the peak, respectively. Then the selective histogram stretching is given by $I(x,y) = (\Lambda - 1) \cdot (I(x,y) - \min)/(\max - \min)$; Λ is the expected maximum intensity level in the histogram-stretched image and $I(x,y)$ is the image function. Fig. 2

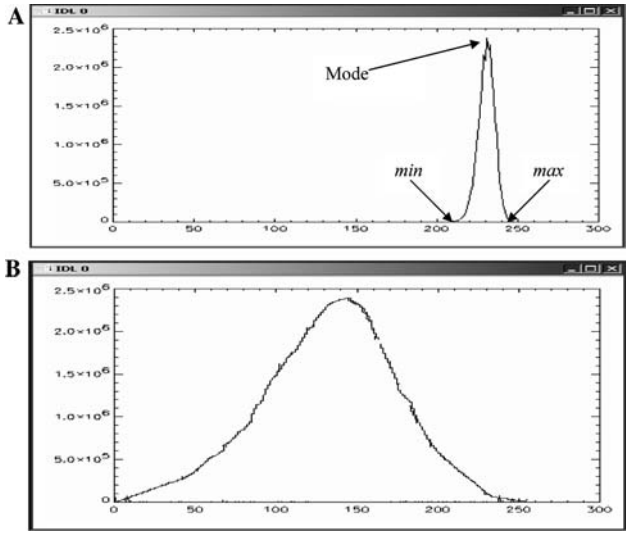

Fig. 2. Histogram of a micrograph (A) before (B) after stretching.

shows, a histogram of a micrograph where the curve falls below 1% of the peak at grey-levels 210 and 250. With offset = 20 and maximum grey scale in a byte image being 255, we use max = 255 and min = 190 for histogram stretching. Since the max and min grey-levels calculated, based on the initial histogram curve, are data dependent, the result of histogram stretching standardizes micrographs by tending to produce a common mean and grey-scale distribution.

Micrographs, in general, have poor signal-to-noise ratio (SNR) as has been stated above. The main type of noise that corrupts micrographs of ice embedded specimens is electron shot noise. In order to increase the SNR, a high degree of smoothing of micrographs is required. Smoothing an image using low pass filters like the Gaussian smoothing filter will also blur the image and compromise the boundary (or the edge) information. What we desire is an image denoising scheme that reduces the background noise and texture variation, while preserving the particle shape boundaries. We employ the non-linear partial differential equation based smoothing technique called the Beltrami flow equation (Sochen et al., 1996, 1998).

Consider the image function $U = I(x, y)$. Linear diffusion can be achieved by a parabolic partial differential equation (PDE), namely

$$I_t = \frac{\partial U}{\partial t} = \frac{\partial^2 U}{\partial x^2} + \frac{\partial^2 U}{\partial y^2}. \tag{1}$$

This process is also called isotropic diffusion. The blurring of important features such as edges that occurs while moving from finer to coarser scales can be avoided by application of anisotropic diffusion methods. The use of diffusion equation for image processing originated with the work of Perona and Malik (1990) where the authors pre-select a diffusion coefficient that preserves the edge information. Image smoothing by way of level set curvature motion (Alvarez et al., 1992; Rudin et al., 1992; Malladi and Sethian, 1996), thwarts the diffusion in the edge direction, thereby preserving the edge information. The main motivation behind the work of Sochen et al. (1996) was to find a natural way of dealing with different types of image mappings, grey scale, color, volumetric etc. The key idea is to view images as embedded maps between two Riemannian manifolds and to define an action potential that provides a measure on the space of these maps. To be specific, let us denote by (Σ, g) the image manifold and its metric, and by (M, h) the image space-feature manifold and its metric, the so-called action potential is the weight of the map $X{:}\Sigma \to M$, i.e.

$$S[X^i, g_{\mu\nu}, h_{ij}] = \int d^m\sigma \cdot g^{\frac{1}{2}} g^{\mu\nu} \partial_\mu X^i \partial_\nu X^j h_{ij}(X), \tag{2}$$

where m is the dimension of Σ, g is the determinant of the image metric, $g^{\mu\nu}$ is the inverse of the image metric, the range of indices is $\mu, \nu = 1, \ldots, \dim \Sigma$ and $i, j = 1, \ldots, \dim M$, and h_{ij} is the metric of the embedding space. This action is the natural generalization of the *L2* norm to non-Euclidean manifolds and is known as the *Polyakov* action (Polyakov, 1981). Minimizing the above potential with respect to the embedding or the feature coordinates leads to different flows that are known in the literature as the Gaussian, curvature flow, etc. We choose a particular minimization, one that sets the first variation of the potential with respect to the embedding to zero. As an example, a grey-level image is an embedding of a surface described as a graph in R^3, as follows: $X : (x, y) \to [x, y, I(x, y)]$ and the metric is defined

$$(g_{\mu\nu}) = \begin{pmatrix} 1 + I_x^2 & I_x I_y \\ I_x I_y & 1 + I_y^2 \end{pmatrix}. \tag{3}$$

The explicit equation describing the smoothing flow is realized by minimizing the action potential with respect to the third coordinate I, namely

$$I_t = \frac{(1 + I_y^2) I_{xx} - 2 I_x I_y I_{xy} + (1 + I_x^2) I_{yy}}{(1 + I_x^2 + I_y^2)^2} \tag{4}$$

with the initial condition $I(x, y, t = 0) = I_0(x, y)$, the original noisy image. By simple algebraic rearrangements of terms in Eq. (4), we can write the flow equation as

$$\frac{\partial U}{\partial t} = (\cos\beta) \cdot \nabla h \cdot \nabla U + (\sin\beta) \cdot h \cdot \nabla^2 U, \tag{5}$$

where the edge indicator function $h = 1/(1 + I_x^2 + I_y^2)$, thus providing a minimum diffusion at the edges and extensive diffusion elsewhere (Malladi and Ravve, 2001, 2002) The first term, $\{(\cos\beta) \cdot \nabla h \cdot \nabla U\}$ is a reaction term responsible for edge-enhancement while the second term $\{(\sin\beta) \cdot h \cdot \nabla^2 U\}$ is a diffusion term responsible for smoothing. β is a parameter that determines the relative contribution of reaction and diffusion terms and varies from 0° to 90°. $\beta = 0°$ is a pure reaction term, $\beta = 45°$ is a non-linear diffusion flow, $\beta = \arctan 2 \approx 63.4°$ is the Beltrami flow (Sochen et al., 1998), and $\beta = 90°$ is the pure diffusion. Thus by suitably selecting β we can achieve desired amount of smoothing without substantially losing edge information. Fig. 3 shows the result of smoothing achieved by the reaction-diffusion technique using different values of β, while parameter such as time step for reaction-diffusion are kept same. We have used $\beta = 75°$. This value is selected experimentally by considering a number of correctly detected particles.

Due to variation in the sample thickness and other factors, micrographs normally show some degree of uneven illumination. Such illumination variation could be corrected by removing low frequency components from the image by high-pass filtering. We have used a rank-leveling approach which is an adoptive high-pass filtering implemented in a mathematical morphology domain (Russ, 1995). In the first step, a background image is constructed by replacing every pixel by the

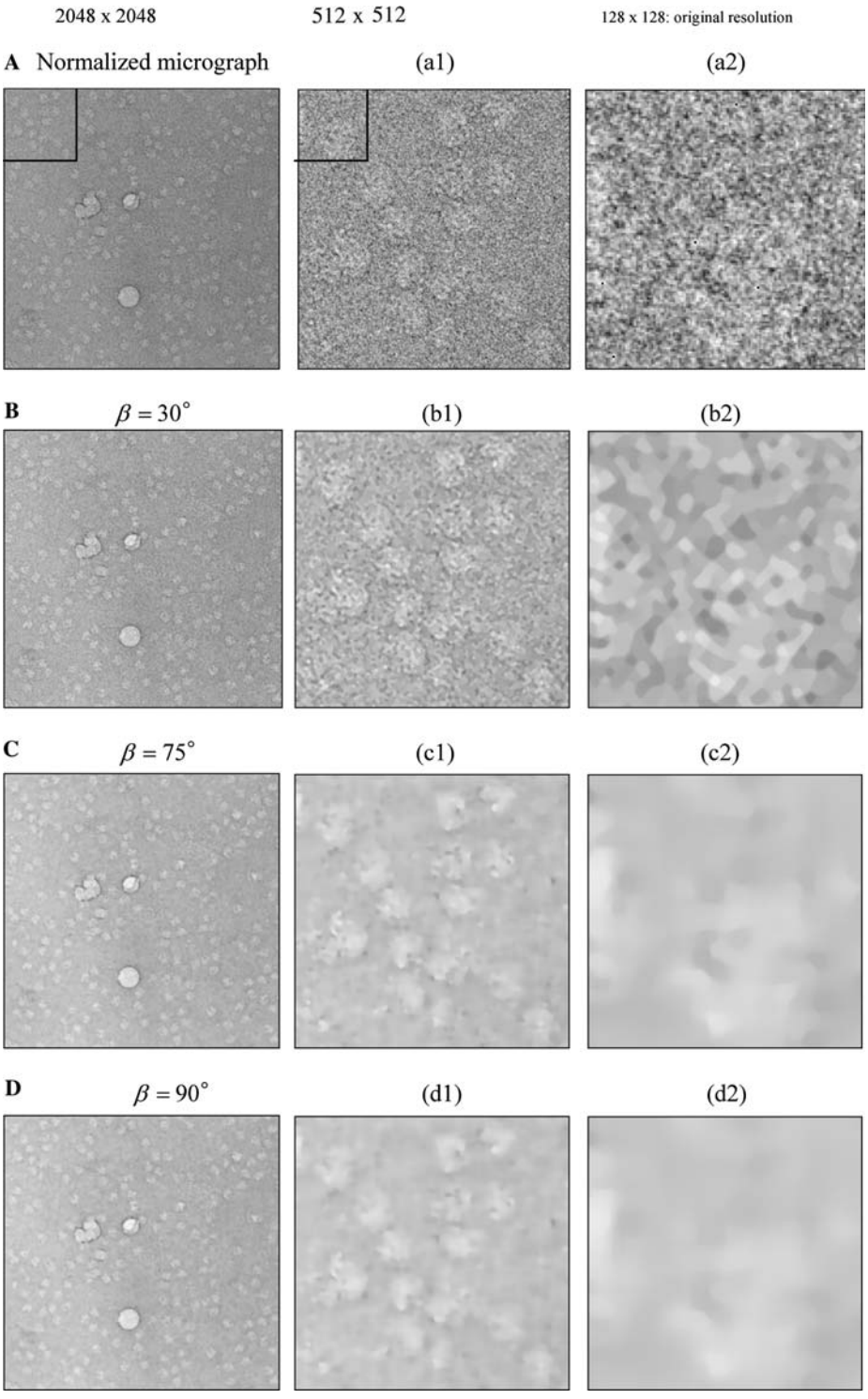

Fig. 3. Effect of changing β in Beltrami-flow based smoothing.

minimum grey-level in its neighborhood (if the particles are brighter than the background) until the objects in the image disappear. The neighborhood size is selected based on the approximate size of the object, i.e., the particle size in the micrograph. If the objects are darker, i.e., have lower grey value than the background, we replace each pixel grey-level by the maximum in its neighborhood. The resulting image is an approximate representation of the background. In the second step, the background image is subtracted from the micrograph, and the grey values below zero are clipped to zero value. Fig. 4, shows the result of pre-processing a

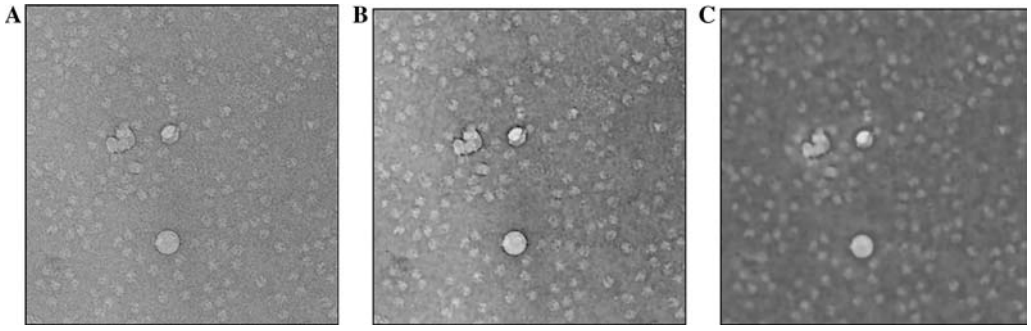

Fig. 4. Result of pre-processing (A) histogram-stretched micrograph, (B) after non-linear smoothing, (C) after rank-leveling.

histogram-stretched micrograph followed by non-linear smoothing and rank-leveling.

2.2. Segmentation of particles

Ideally, a segmentation method finds those sets of pixels that correspond to distinct structures or regions of interest in the image and gives a unique label to each individual set. Segmentation of complex images involves several stages such as thresholding to separate background from foreground, distinguishing artifacts from objects, edge and/or region based algorithms to separate objects which are touching or closely located, component labeling and tuning the boundary pixel location for better precision.

2.2.1. Thresholding

Thresholding is a conversion from a grey-level image to a bi-level image. A bi-level image should contain all the information concerning the number, position, and structure of the objects that are present in the grey-level image while containing much less other information. The problem is to select a proper threshold that accomplishes the above task. We have observed that selection of a single threshold for an entire micrograph is not possible in most of the cases due to overlapping of the grey-levels of the particles and background from different regions of the image. The first issue that must then be addressed, if regional thresholds are to be used, is to determine how many thresholds are needed and what the sizes of the regions are. We have implemented an adaptive region selection method. In the first step, the image is amplitude thresholded at a global mean intensity value $(k \cdot \mu)$, where k is a tuning parameter and μ is the mean intensity of the pre-processed micrograph. All connected components in the foreground are identified by component labeling (Dillencourt et al., 1992). Each such connected component is then considered as an individual region. In the second step, the mean grey-level μ_i of connected component i is calculated. Connected component i is further thresholded at a unique threshold value $(k_1 \cdot \mu_i)$. The tuning factor k_1 is experimentally set (we have used $k = 1.0$ and $k_1 = 0.5$).

Bi-level micrographs thus obtained still contain many artifacts in the form of tiny isolated structures and small holes within the particles which are dealt with in the following way. Using a circular structuring element (Serra, 1982), the thresholded micrograph is 'opened.' If S is the structuring element and A is the image then grey-scale opening of A by S is defined as $S \oplus \{S \Theta A\}$; where,

$$S \Theta A = \min\{A[i-r, j-c] - S[r,c][i-r, j-c] \in A[r,c] \in S\}$$

$$S \oplus A = \max\{A[i-r, j-c] + S[r,c][i-r, j-c] \in A[r,c] \in S\};$$

$\oplus$ is the dilation operator and Θ is the erosion operator. This opening operation reduces small noisy objects that resulted from thresholding micrographs that are still somewhat textured. Following this, a closing operation $S \Theta \{S \oplus A\}$, reduces noisy holes in the particles. The structural smoothing due to morphological filtering also force the objects to have a convex shape that can be better segmented. Fig. 5 shows the result of multi-level, region-based thresholding followed by morphological opening and closing.

2.2.2. Relative feature filtering

Once the binarization process described above has been completed, it is still necessary to distinguish artifacts from individual particles and/or clusters of parti-

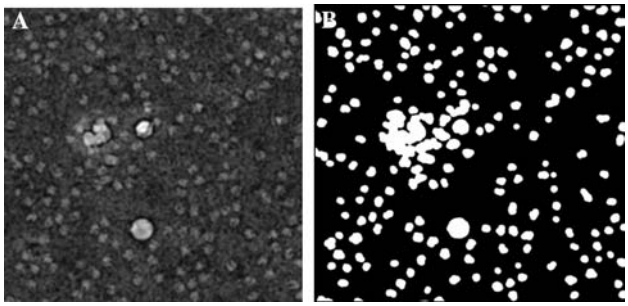

Fig. 5. (A) Part of the pre-processed image. (B) After thresholding and noise removal by morphological filters.

cles in the image. The use of some simple and intuitively obvious filters such as relative size and the relative average intensity of pixels within the candidate particle are recommended for this purpose. When the size and the average intensity values of the particles in the micrograph are known, this information can be provided as a priori information to the filtering process for selecting individual isolated particles and flagging cluster of particles for further processing. Otherwise a data-driven process to filter-out the artifacts is recommended. We have tested one such approach in which the relative size of the object r_v defined as the ratio of the size of that object to the average size of objects in the image, is used to eliminate artifacts. Particles are first ordered based on their sizes, i.e., number of pixels within the particles. The average size is calculated by an α-trimmed filter which excludes α number of extreme size elements in the size ordered list of objects for calculation of the average object size in the image (Oten, 2000). We have excluded 25% of the particles on both extremes of the ordered list of particles. If the size of the object i is V_i, then the relative size of the object i is given by:

$$r_{v_i} = \frac{V_i}{\frac{1}{(N-2\alpha)} \cdot \sum_{k=\alpha}^{N-\alpha} V_k}, \tag{6}$$

where N is the number of isolated objects present in the image and α is the cut-off threshold of α-trimmed filter. The relative intensity of the object r_{I_i} is defined as the ratio of the average intensity of the object pixels to the average intensity of foreground pixels in the image. If the average intensity of the object i is $\overline{I}_i$, then

$$r_{I_i} = \frac{\overline{I}_i}{\frac{1}{(N-2\alpha)} \cdot \sum_{k=\alpha}^{N-\alpha} (\bar{I}_k)}. \tag{7}$$

All those particles with relative average intensity less than 0.3 or relative size less than 0.5 are considered as artifacts and eliminated. Fig. 6A is a normalized micrograph, Fig. 6B, shows a thresholded image while Fig. 6C displays all the isolated individual ribosome particles. In addition, objects with relative mean object size more than 1.5 and less than 3.0 are considered as possible clusters of two or three particles and are flagged-off for further segmentation. Objects with relative size more than 3.0 are eliminated from further processing. Fig. 6D shows the image that has been flagged-off for further segmentation which we call the "residue image."

2.2.3. Cluster segmentation

The residue-image, consisting of particle clusters flagged-off by relative feature filtering, is labeled using a component labeling algorithm. Segmentation of clusters is done in two independent stages.

Stage 1: the foreground of the residue-image is eroded one pixel thickness at a time. Ideally, this erosion process continues until a unique marker is obtained for each particle in the region of interest. Markers are the small group of connected pixels located at the approximate center of individual particles. The markers are tagged with a unique label and the number of erosion iterations needed to bring it to marker size. In the second step, markers are subject to controlled dilation. Markers are grown into their neighboring background pixels under certain conditions.

- No two growing markers are allowed to overlap or touch one another.
- The growing process is terminated when the grown region covers all the foreground pixels in the original residue-image.

A pixel level logical AND operation between the residue image and the dilated markers image provides segmentation of many particles in the cluster. The relative size filter with feature parameters obtained from already isolated particles can then be used to extract particles that are isolated by the erosion-dilation process.

Stage 2: if there are clusters of particles still left in the residue-image, then a final step of segmentation based on region growing over a distance map, which is a generalized version of the watershed technique, is applied (Umesh Adiga and Chaudhuri, 2001; Vincent and Soille, 1991). A distance map of the residue-image is generated using the Borgefors algorithm (Borgefors, 1996). Homogeneous regions in the distance map are identified and the distance values of those pixels are rescaled to reduce flat fields (Bleu and Joshua, 2000).

Let *dist(.)* represent the distance value of pixels in the distance map.

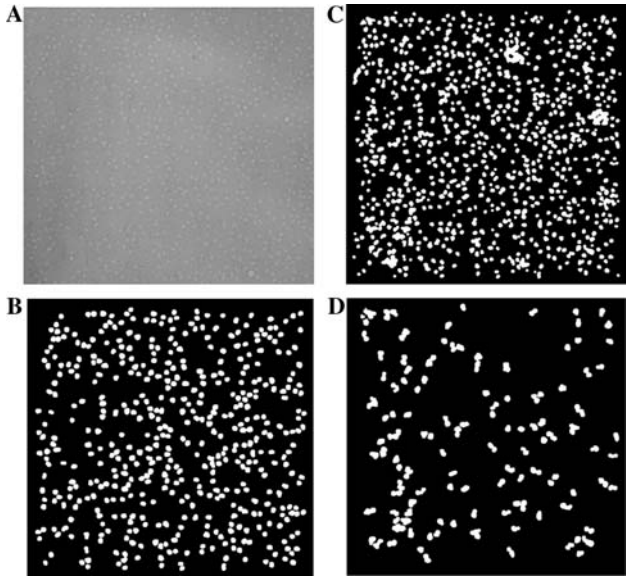

Fig. 6. (A) Normalized micrograph. (B) After binarization. (C) Objects isolated as individual particles. (D) Objects flagged-off as cluster of particles. Note that the larger white "clumps" in (B) have been eliminated from (C) and (D) by relative size filtering.

Step 1: connected group of pixels having maximum distance d_{max} in the distance map are considered as markers. A marker may consist of single pixel or a group of connected pixels. The markers are labelled by the component labelling algorithm. Let d_{max} be the maximum distance in the distance map, d_{next} is the next maximum distance level, and d_{min} is the minimum distance value in the distance map.

Step 2: pixels having a distance value (d_{next}) and located in the immediate neighborhood of the labelled regional markers are merged with their neighboring regional marker. This step can also be viewed as growing markers into their neighborhood pixels that have a distance value d_{next} by reassigning their distance values to be d_{max} and tagging them with the corresponding label of the marker.

The isolated pixel or group of connected pixels in the distance map with distance d_{next} and not having a labelled regional marker in their immediate neighborhood are considered as new markers and given a new unique label as well as having its distance value upgraded to d_{max}.

Step 3: $d_{next} =$ next maximum distance value in the image which is less than d_{max}.

Step 4: if the $d_{next} \neq d_{min}$ then steps 2 and 3 are repeated.

The resulting image is filtered using relative size filters. Fig. 7, shows an example of segmentation of clusters of ribosome particles.

A second stage of analysis is necessary to identify missed ribosome particles in the first stage. Every segmented particle projection in the original unprocessed micrograph is replaced by a background texture patch. The resulting image is then considered as a new, preprocessed micrograph, and all the steps of segmentation are applied again. As most of the parameters controlling segmentation are data driven, it is not necessary to retune them at this intermediate stage. Particles thus extracted are added to the original set of segmented particles. Fig. 8 shows the result of second stage analysis to pick particles that were left-out in the first stage. We have observed that about 10–15% of the total particles segmented are obtained from the second stage of processing. The increase in number of false positives due to the second stage of processing is negligible.

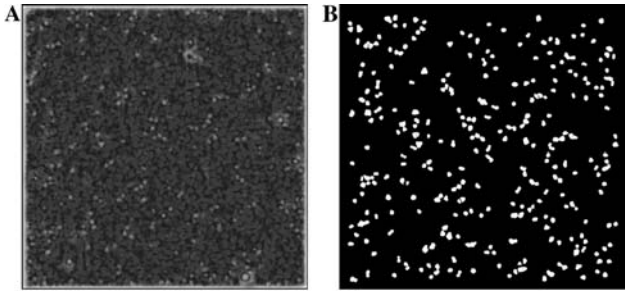

Fig. 8. Illustration of second stage of particle picking. (A) Pre-processed micrograph after replacing all the particle area by a grey value less than the mean grey value of the pre-processed micrograph. (B) Particles and particle clusters picked during the second stage only.

Our aim is to extract each particle as a small sub-image. All the sub-images should have the same size (same number of columns and rows) so that they can be used for further analysis towards 3-D construction. To accomplish this, the centroid of each particle that is segmented from the micrograph is calculated, and a fixed size box is stamped around the centroid such that the complete particle is enclosed within the box. Fig. 9 shows an example of a micrograph where segmented ribosome particles are boxed.

3. Experimental results and discussion

The basic idea behind this methodology for picking ribosome particles is to pre-process the image to an extent that the standard segmentation algorithms can successfully identify each particle in the image. A two tone version of the image is then used to measure the size (i.e., the area) of the particles and the average density within this area is further used to identify the particles. Our goal is to consistently achieve, on a large set of data, 80% efficiency with respect to manual selection, with less than 10% false positives contained in the data set, and to do so without human intervention. Table 1 gives a quantitative analysis of the efficiency of

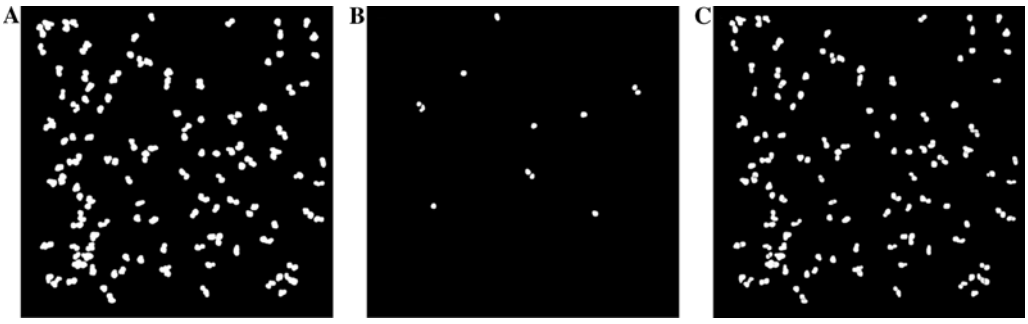

Fig. 7. (A) Same as Fig. 6C, (B) result of erosion-dilation, (C) result of region growing/watershed on a distance map for segmentation of clusters.

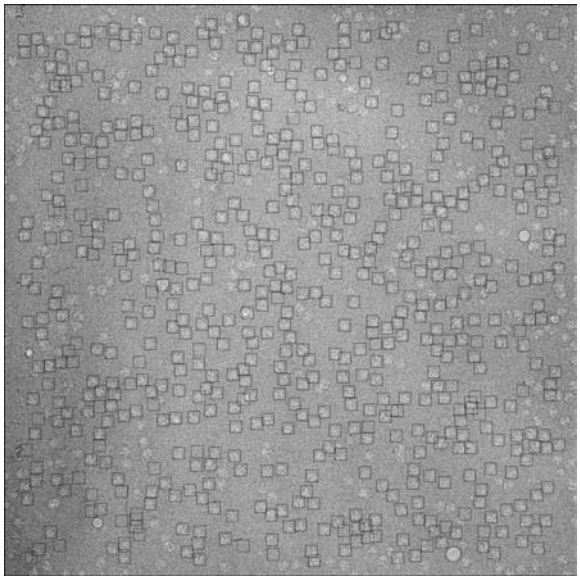

Fig. 9. Illustration of boxing of recognized ribosome particles. Most of the apparent ribosome particles that can still be seen without boxes are, in fact, particles that are not picked by human either.

our automatic procedure in the case of a few micrographs with routine image quality. We have achieved and in most cases exceeded the expected target of 80% recognition with less than 10% false positives. The efficacy of our approach needs to be further tested on a large number of micrographs before accepting the software as a routine tool for picking ribosome particles.

The image files Smic01.spi, Smic02.spi, and Smic03.spi, with particle coordinates that are known from manual boxing, were used as gold standards to test the performance of the protocol and to establish the parameter values used in the algorithm. The number of particles that were boxed both manually and automatically was used to compute the efficiency of the software with respect to the manual boxing process. If $\Theta_{\text{man}} = \{p_1, p_2, \ldots, p_n\}$ is the set of manually boxed particles, where the size of the set $\#\{\Theta_{\text{man}}\} = n$, and $\Theta_{\text{aut}} = \{p_1, p_2, \ldots, p_m\}$ is the set of particles boxed automatically, where $\#\{\Theta_{\text{aut}}\} = m$, then $\{\Theta_{\text{man}} \cap \Theta_{\text{aut}}\}$ is the set of particles that are picked by both automatic and manual methods. The symbol '$\cap$' is the set intersection that brings out those elements that are common to both sets. The set $\{\Theta_{\text{man}} \setminus \{\Theta_{\text{man}} \cap \Theta_{\text{aut}}\}\}$ is the set of particles that are manually picked but not picked up by the software. The symbol '$\setminus$' denotes the set difference. The set, $\{\Theta_{\text{aut}} \setminus \{\Theta_{\text{man}} \cap \Theta_{\text{aut}}\}\}$ is the set of false positives, i.e., set of particles boxed by the automatic method while rejected as non-particles by the manual method. The percentage efficiency of the automatic method is then calculated by % efficiency $= (\#\{\Theta_{\text{man}} \cap \Theta_{\text{aut}}\}/n) \times 100$. The particles that are marked by the automatic process but not by manual boxing are considered to be false positives. The efficiency of automatic particle picking, as defined above, is calculated based on the total number of false positives listed in column 5 rather than the estimated number listed in column 6 of Table 1. The column "estimated false positives" is provided because some of the boxes that are marked by the software, but not by the manual process, appeared to have actual particles in them.

Increasing β increases the diffusive property of the anisotropic diffusion process. An optimal trade-off between protecting the boundary of the particles, and smoothing the noisy texture in the interior of the particles as well as in the image background, is achieved by trial-and-error. This trade-off resulted in our choice of $\beta = 75°$ as a default value, as it produced a marked reduction in the already small percentage of false positives with only a modest loss in the recognition of true positives. Table 2 shows the effect of using different values of β in the Beltrami flow based pre-processing. Selection of the threshold value for binarization is a fairly robust process. Thresholding at the average brightness in the first stage and calculating unique thresholds for

Table 1
Quantitative analysis of manual particle picking and automatic method

No.	Image name	No. of particles manual	No. of particles automatic	False positives	Estimated false positives	% recognition/ efficiency
1	Smic01	591	583	25	11	94%
2	Smic02	645	596	21	8	89%
3	Smic03	634	521	18	14	80%

Table 2
Effect of the smoothing parameter on particle picking

Image name	Manual pick	PDE $\beta = 30°$ count/false +ve	PDE $\beta = 45°$ count/false +ve	PDE $\beta = 62.3°$ count/false +ve	PDE $\beta = 75°$ count/false +ve	PDE $\beta = 90°$ count/false +ve
Smic01	591	533/71	589/64	646/57	583/25	484/28
Smic02	645	513/51	546/48	558/45	596/21	433/30
Smic03	634	598/81	580/58	601/47	521/18	455/31

subsequent regions formed by first stage of thresholding is a novel approach towards region selection in region based thresholding. Since the selective histogram stretching standardizes average brightness and histogram shape of all the micrographs, retuning of pre-processing and segmentation parameters is not necessary while working on different micrographs. In cases where the binarization does not produce enough single-particle signatures, a simple rearrangement of the steps, i.e., performing cluster segmentation on the binarized data before relative size filtering would reduce the necessity of tuning filter parameters. Thus, the software is more-or-less independent of parameter tuning while operating on a set of micrographs obtained under similar settings.

It has been observed that our software performs with a better computational efficiency when the images are of size, say, 1024×1024, rather than when they are 4096×4096 and above. This is an issue of implementation of the algorithms and the efficiency of the computer. To make our software work efficiently for a large image on smaller machines such as PC, etc., a divide and conquer method can be adopted. The large image is divided into optimum size for the software to run efficiently on each image part. When each image part is processed, however, we reject those particles that are too close to the image border. For example, when an image of 4096×4096 pixels is divided into 16 parts of size 1024×1024, a large number of particles in each part would be rejected as being too close to the border. This problem can be solved by not rejecting any objects until the whole image is reconstructed by tiling individual, processed/segmented, image parts.

To complete all stages of automatic particle picking on a 2048×2048 image with about 600 particles, the program took 21 min on a 1 GHz/256 Mb PC with Win2000 operating system. The program is implemented in Interactive Data Language (www.rsi.com). Re-implementing it in C or C++ would improve the efficiency at least by 50%. The efficiency of the program is also directly related to the quality of the image and the number of single isolated particles present, as well as the number of particle clusters present.

An important difference from the existing methods of particle selection is that this method can be defined as blind, as no manual intervention is allowed. The high degree of accuracy achieved in particle selection is due to extensive pre-processing that improves the particle contrast from its background. The application of the PDE-based Beltrami flow equation for smoothing and enhancing features helps in retaining the particle boundary, which in turn preserves the particle size and shape. Though the program was tested on relatively similar data sets, we expect it to work generally well on all micrographs acquired with similar instrument settings. Under different settings, retuning of one or several parameters may be necessary.

Acknowledgments

We would like to thank Dr. Kenneth Downing, Dr. Eva Nogales, and Dr. Joachim Frank for important discussions and advice. Dr. William Nicholson provided key support in earlier stages of the related work that lead up to the approach reported here. This work has been supported by the Director, Office of Science, US Department of Energy Contract No. DE-AC03-76SF00098; NIH Grant GM62989; and a grant from the Agouron Foundation.

References

Alvarez, L., Lions, P.L., Morel, J.M., 1992. Image selective smoothing and edge detection by non-linear diffusion (II). SIAM J. Numer. Anal. 29, 845–866.

Bleu, A., Joshua, L.L., 2000. Watershed based segmentation and region merging. Comput. Vision Image Understanding 77, 317–370.

Borgefors, G., 1996. On digital distance transforms in three dimensions. Comput. Vision Graph. Image Process. 64, 368–376.

Dillencourt, M.B., Samet, H., Tamminen, M., 1992. Corrigenda: a general approach to connected component labeling for arbitrary image representations. J. ACM 39, 985–986.

Frank, J., 1996. Three-dimensional Electron Microscopy of Macromolecular Assemblies. Academic Press, San Diego.

Glaeser, R.M., 1971. Limitations to significant information in biological electron microscopy as a result of radiation damage. J. Ultrastruct. Res. 36, 466–482.

Henderson, R., 1995. The potential and limitations of neutrons, electrons and X-rays for atomic resolution microscopy of unstained biological molecules. Q. Rev. Biophys. 28, 171–193.

Lata, K.R., Penczek, P., Frank, J., 1995. Automatic particle picking from electron micrographs. Ultramicroscopy 58, 381–391.

Malladi, R., Ravve, I., 2002. Fast difference schemes for edge enhancing Beltrami flow. In: Heyden, et al. (Eds.), Computer Vision ECCV 2002, vol. LNCS 2350, pp. 343–357.

Malladi, R., Ravve, I., 2001. Fast difference scheme for anisotropic Beltrami smoothing and Edge contrast enhancement of Gray level and Color images. LBNL. Tech Report-48796. Lawrence Berkeley National Laboratory, University of California, Berkeley.

Malladi, R., Sethian, J.A., 1996. Image processing: flown under min/max curvature flow and mean curvature. Graph. Models Image Process. 58, 127–141.

Nicholson, W.V., Glaeser, R.M., 2001. Review: automatic particle detection in electron microscopy. J. Struct. Biol. 133, 90–101.

Oten, R., 2000. Nonlinear signal and image processing based on order statistics, Ph.D. thesis, University of California, Irvine.

Perona, P., Malik, J., 1990. Scale space and edge detection using anisotropic diffusion. IEEE Trans. Pattern Anal. Mach. Intell. 12, 629–639.

Polyakov, A.M., 1981. Quantum geometry of bosonic strings. Phys. Lett. B 103 (3), 207–210.

Rudin, L., Osher, S., Fatemi, E., 1992. Nonlinear total variation based noise removal algorithms. Physica D 60, 259–268.

Russ, J.C., 1995. The Image Processing Handbook. CRC Press, London.

Sali, A., Glaeser, R.M., Earnest, T., Baumeister, W., 2003. From words to literature in structural proteomics. Nature 422, 216–225.

Serra, J., 1982. Image Analysis and Mathematical Morphology. Academic Press.

Sochen, N., Kimmel, R., Malladi, R., 1996. From High Energy Physics to Low Level Vision, LBNL report #39243, Lawrence Berkeley National Laboratory, University of California, Berkeley, USA.

Sochen, N., Kimmel, R., Malladi, R., 1998. A general framework for low level vision. IEEE Trans. Image Process., special issue on PDEs and Geometry-Driven Diffusion in Image Processing and Analysis 7, 310–318.

Umesh Adiga, P.S., Chaudhuri, B.B., 2001. An efficient method based on watershed and rule based merging for segmentation of 3-D histo-pathological images. Pattern Recogn. 34, 1449–1458.

Vincent, L., Soille, P., 1991. Watersheds in digital spaces: an efficient algorithm based on immersion simulations. IEEE Trans. Pattern Anal. Mach. Intell. 13, 583–593.